

Direct Detection Constraints on Blazar-Boosted Dark Matter

Jin-Wei Wang,^{*} Alessandro Granelli,[†] and Piero Ullio[‡]

*Scuola Internazionale Superiore di Studi Avanzati (SISSA), via Bonomea 265, 34136 Trieste, Italy
INFN, Sezione di Trieste, via Valerio 2, 34127 Trieste, Italy and
Institute for Fundamental Physics of the Universe (IFPU), via Beirut 2, 34151 Trieste, Italy.*

We explore the possibility that relativistic protons in the extremely powerful jets of blazars may boost via elastic collisions the dark matter particles in the surroundings of the source to high energies. We concentrate on two sample blazars, TXS 0506+056 — towards which IceCube recently reported evidence for a high-energy neutrino flux — and BL Lacertae, a representative nearby blazar. We find that the dark matter flux at Earth induced by these sources may be sizeable, larger than the flux associated with the analogous process of DM boosted by galactic cosmic rays, and relevant to access direct detection for dark matter particle masses lighter than 1 GeV. From the null detection of a signal by XENON1T, MiniBooNE, and Borexino, we derive limits on dark matter-nucleus spin-independent and spin-dependent cross sections which, depending on the modelization of the source, improve on other currently available bounds for light DM candidates of one up to five orders of magnitude.

Introduction— The nature of dark matter (DM) in the Universe remains elusive [1, 2]. Steady progresses have been made in the attempt to identify the DM particles forming the Milky Way (MW) halo by detecting their elastic scattering of target nuclei, such as, most recently, by XENON1T [3, 4] and PandaX-II [5]. A limitation of such direct detection technique is the fact that MW DM particles are expected to have small velocities, typically $\sim 10^{-3}c$, and hence nuclear recoil energies exceed detector thresholds, say ~ 1 keV, only for DM masses $\gtrsim 1$ GeV.

In the latest years a few scenarios with “boosted” DM populations have been proposed, allowing for nuclear recoil signals even for lighter DM particles, see, e.g., Refs. [6–9]. In Ref. [10] the authors consider the interesting possibility that MW DM particles are boosted via elastic scatterings with galactic high-energy cosmic rays, deriving relevant constraints for sub-GeV DM candidates. We propose here blazars as ideal DM boosters: they are associated to intense sources of high-energy non-thermal particles, they are located in a gravitational potential with a supermassive Black Hole (BH) at the center, whose formation may have triggered a large enhancement of the ambient DM density, and they are relatively close to us.

Blazars are a type of Active Galactic Nuclei (AGN) accelerating particles into two back-to-back jets, with one of them in close alignment to our line of sight (LOS) [11]. They are characterized by a non-thermal continuous photon Spectral Energy Distribution (SED) with two peaks, one in the infrared/X-ray bands and the other at γ -ray frequencies [12]. Models of the SED [13–19] have been refined with GeV-TeV data from Fermi-LAT and Air Cherenkov Telescopes [20, 21]: it is widely accepted that the low-energy peak is due to synchrotron emission by electrons, but there is still no consensus on the origin of the high-energy component. While electrons could also be responsible for it (leptonic models), a highly-relativistic population of protons may also be

present in the jets and account for the γ -ray emission (pure hadronic and hybrid lepto-hadronic models, see, e.g., [22] for a recent model review). Moreover, given the high variability of blazars (both in time and population), the parameters of each model, as well as the goodness of the fit, strongly depend on the considered source and the time of observation. It is therefore complicated to establish a unifying picture.

Multimessenger astrophysics can provide more insights into the physics of blazar jets. Recently, compelling evidence of high-energy cosmic neutrinos from the blazar TXS 0506+056 was found by the IceCube Neutrino Observatory [23–25]. Studies of the SED have shown that the lepto-hadronic model, although slightly contrived in terms of proton luminosities, is in general adequate to explain both the detected neutrino flux and the γ -ray emission of TXS 0506+056 [26–31].

Electrons and protons in the jets of a blazar can collide with ambient DM particles. Scatterings off DM by electrons and protons in the jet plasma of AGN were already considered in Refs. [32, 33], where the authors focused on photon emissions. Instead, in the present paper, similarly to the acceleration mechanism due to cosmic rays [10], we consider DM boosted by protons in the jet of blazars, derive the induced DM flux at Earth and compute the associated nuclear recoil direct detection signal. We refer to DM boosted via this mechanism as Blazar-Boosted Dark Matter (BBDM). Motivated by IceCube observations, we decide to focus our study on the blazar TXS 0506+056. For comparison, we also consider the near representative blazar BL Lacertae. We then discuss the implications the non-detection of BBDM from the two sources have on spin-independent and spin-dependent DM-nucleus cross sections. An analogous analysis dedicated to leptophilic DM, for which boosting by electrons in the jet and scattering off electrons in the detector are relevant, is postponed to a future related study.

Spectrum of the relativistic blazar jet– We consider the simplifying assumption that the blazar emission originates from a homogeneous zone (blob) in the jet where particles (mainly electrons and protons) are distributed isotropically [34]. The blob, as seen by an observer standing still with respect to the BH center-of-mass, propagates with speed β_B along a direction (jet axis) inclined with respect to the observer’s LOS by an angle θ_{LOS} . The corresponding Lorentz boost factor is $\Gamma_B \equiv (1 - \beta_B^2)^{-1/2}$.

For the (lepto-)hadronic models, the energy spectrum of protons in the blob frame fulfills a single power-law distribution:

$$\frac{d\Gamma'_p}{dE'_p d\Omega'} = \frac{1}{4\pi} c_p \left(\frac{E'_p}{m_p} \right)^{-\alpha_p} \quad (1)$$

with $\gamma'_{\min,p} \leq E'_p/m_p \leq \gamma'_{\max,p}$. The normalisation constant c_p can be computed from the proton luminosity L_p [33]. The proton spectrum in the observer’s rest frame can then be rewritten as (see Supplemental Material)

$$\begin{aligned} \frac{d\Gamma_p}{dT_p d\Omega} &= \frac{1}{4\pi} c_p \left(1 + \frac{T_p}{m_p} \right)^{-\alpha_p} \\ &\times \frac{\beta_p (1 - \beta_p \beta_B \mu)^{-\alpha_p} \Gamma_B^{-\alpha_p}}{\sqrt{(1 - \beta_p \beta_B \mu)^2 - (1 - \beta_p^2)(1 - \beta_B^2)}}, \end{aligned} \quad (2)$$

where $T_p \equiv E_p - m_p$ is the proton kinetic energy, $m_p \simeq 0.938$ GeV is the proton mass, $\beta_p = [1 - m_p^2/(T_p + m_p)^2]^{1/2}$ is the proton speed. Given a SED, the minimal and maximal Lorentz boost factors, i.e. $\gamma'_{\min,p}$ and $\gamma'_{\max,p}$, the power-law index α_p , the Doppler factor $\mathcal{D} = [\Gamma_B (1 - \beta_B \cos \theta_{\text{LOS}})]^{-1}$, and the luminosity L_p are fitted. Two common assumptions in the fit are $\mathcal{D} = 2\Gamma_B$ and Γ_B , corresponding to, respectively, $\theta_{\text{LOS}} = 0$ and $1/\mathcal{D}$ (with $\mathcal{D} \gg 1$). We use the results presented in Refs. [27, 28] for TXS 0506+056 and [19] BL Lacertae, summarised in Table I. In the same table we include the redshift z [35, 36], the luminosity distance d_L , and BH mass M_{BH} (in units of solar masses M_\odot) [37, 38], as they are relevant in the next sections.

In Fig. 1 we show the spectrum of protons from the source TXS 0506+056, for the parameters given in Table I and different polar angles. For the high-energy region ($T_p \gg m_p$), the spectra are parallel because $d\Gamma_p/(dT_p d\Omega) \propto T_p^{-\alpha_p}$ (see Eq. (2)), while for the low-energy region ($T_p \ll m_p$), we have $d\Gamma_p/(dT_p d\Omega) \approx c_p \Gamma_B^{-\alpha_p} (4\pi \beta_B)^{-1} \sqrt{2T_p/m_p}$. The peak that appears in the curve for $\theta = 0^\circ$ corresponds to the kinetic energy of a proton that is at rest in the blob frame, i.e. $T_p = m_p(\Gamma_B - 1)$. The spectrum of BL Lacertae is qualitatively similar.

Dark matter density profile– The adiabatic growth of a BH in the central region of a DM halo is expected

| (Lepto-)Hadronic Model Parameters | | |
|-----------------------------------|------------------------|----------------------|
| Parameter (unit) | TXS 0506+056 | BL Lacertae |
| z | 0.337 | 0.069 |
| d_L (Mpc) | 1835.4 | 322.7 |
| $M_{\text{BH}} (M_\odot)$ | 3.09×10^8 | 8.65×10^7 |
| \mathcal{D} | 40* | 15 |
| Γ_B | 20 | 15 |
| $\theta_{\text{LOS}} (^\circ)$ | 0 | 3.82 |
| α_p | 2.0* | 2.4 |
| $\gamma'_{\min,p}$ | 1.0 | 1.0 |
| $\gamma'_{\max,p}$ | $5.5 \times 10^{7*}$ | 1.9×10^9 |
| L_p (erg/s) | $2.55 \times 10^{48*}$ | 9.8×10^{48} |

TABLE I. The model parameters for the blazars TXS 0506+056 (Lepto-Hadronic) [27, 28] and BL Lacertae (Hadronic) [19] used in our calculations. The quantities flagged with a star (*) correspond to mean values computed from the ranges given in the second column of Table 1 of Ref. [28]. In the model fitting, the assumption of $\mathcal{D} = 2\Gamma_B$ (Γ_B) is used for TXS 0506+056 (BL Lacertae).

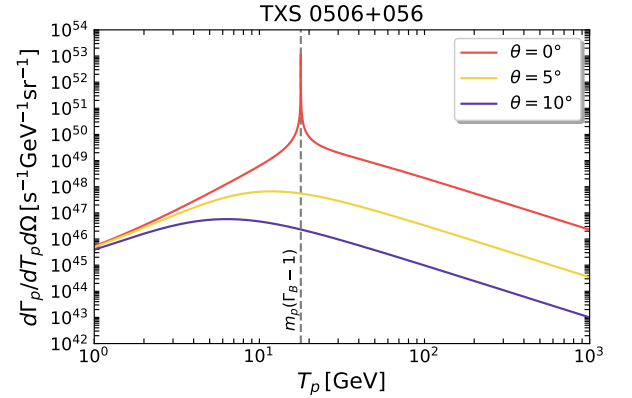


FIG. 1. The spectrum of protons in the observer’s frame for TXS 0506+056. The model parameters used are given in Table I. The different colours correspond to different polar angles: $\theta = 0^\circ$ (red), 5° (yellow), and 10° (purple). The vertical grey dashed line corresponds to a proton kinetic energy of $T_p = m_p(\Gamma_B - 1)$.

to focus the distribution of DM particles, giving rise to a very dense spike. The phenomena was first discussed by Gondolo and Silk [39], who used adiabatic invariants to show that a pre-existent self-gravitating spherical DM profile, with power-law scaling $\rho(r) \propto r^{-\gamma}$, close to the BH is modified into the steeper profile:

$$\rho'(r) \propto r^{\frac{9-2\gamma}{4-\gamma}}. \quad (3)$$

While the normalization and radial extension for the spike can be explicitly derived in terms of the normalization of the profile before the BH growth and the BH mass M_{BH} , in general one finds that the amount of DM which is displaced to form the spike is about the same as M_{BH} , see also Ref. [40]. In the following we will consider

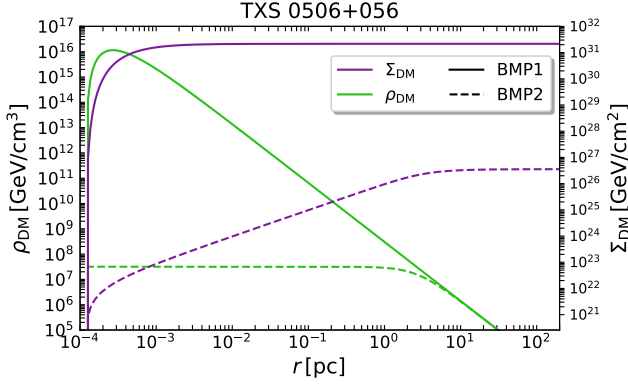


FIG. 2. The distribution of Σ_{DM} (purple) and ρ_{DM} (green) for TXS 0506+056 with $m_\chi = 1$ MeV. The solid and dashed styles correspond to BMP1 and BMP2, respectively.

$\gamma = 1$ (matching the central scaling of the Navarro-Frenk-White profile, motivated by N-body simulations in cold DM cosmologies) and fix the normalization via:

$$\int_{4R_S}^{10^5 R_S} 4\pi r^2 \rho'(r) dr \simeq M_{\text{BH}}. \quad (4)$$

In this expression R_S is the Schwarzschild radius, and the integral extends from $4R_S$, the radius at which the DM profile goes to zero because of capture onto the BH, to $10^5 R_S$, a typical size for the adiabatically contracted spike. In frameworks with DM candidates that can annihilate in pairs, such as, e.g., thermal relics from the early Universe, there is a maximal DM density compatible with annihilations, about $\rho_{\text{core}} \simeq m_\chi / (\langle \sigma v \rangle_0 t_{\text{BH}})$, where $\langle \sigma v \rangle_0$ is the DM annihilation cross section times relative velocity and t_{BH} is the time since the BH formed. This may then induce an inner “flattening” of the profile:

$$\rho_{\text{DM}}(r) = \frac{\rho'(r) \rho_{\text{core}}}{\rho'(r) + \rho_{\text{core}}}. \quad (5)$$

Avoiding to focus on specific models, in the following we will refer to two benchmark points (BMPs):

BMP1) $\langle \sigma v \rangle_0 = 0$, so that $\rho_{\text{core}} \rightarrow +\infty$ and $\rho_{\text{DM}} = \rho'$;

BMP2) $\langle \sigma v \rangle_0 = 10^{-28} \text{ cm}^3 \text{ s}^{-1}$ and $t_{\text{BH}} = 10^9 \text{ yr}$;

where the case with $\langle \sigma v \rangle_0 = 0$ would be appropriate, e.g., for asymmetric DM models. The corresponding profiles are shown in Fig. 2 together with the LOS integral:

$$\Sigma_{\text{DM}}(r) \equiv \int_{4R_S}^r \rho_{\text{DM}}(r') dr'. \quad (6)$$

Σ_{DM} , the relevant quantity for the BBDM signal, tends to saturate at $r \gtrsim 10 \text{ pc}$; a different choice of γ or the upper limit of integration $10^5 R_S$ would have a marginal impact.

Dark matter flux from blazars– The DM particles can be boosted up to high energies due to elastic scatterings with relativistic protons in the jet. Assuming an isotropic scattering (in the center-of-mass rest frame) and neglecting DM motion with respect to protons, the BBDM flux per kinetic energy reads

$$\frac{d\Phi_\chi}{dT_\chi} = \frac{\Sigma_{\text{DM}}^{\text{tot}} \tilde{\sigma}_{\chi p}}{2\pi m_\chi d_L^2} \int_0^{2\pi} d\phi_s \int_{T_p^{\min}(T_\chi)}^{T_p^{\max}} \frac{dT_p}{T_\chi^{\max}(T_p)} \frac{d\Gamma_p}{dT_p d\Omega}, \quad (7)$$

where ϕ_s is the azimuth with respect to the LOS, T_χ^{\max} the maximal DM energy after scattering and $\Sigma_{\text{DM}}^{\text{tot}} \equiv \Sigma_{\text{DM}}(r \gg 10 \text{ pc})$; also, we assume:

$$\tilde{\sigma}_{\chi p} = \sigma_{\chi p} G^2 (2m_\chi T_\chi / \Lambda_p^2), \quad (8)$$

where $\sigma_{\chi p} \in \{\sigma_{\chi p}^{\text{SI}}, \sigma_{\chi p}^{\text{SD}}\}$ is the zero-momentum transfer spin-independent or spin-dependent cross section and the form factor $G(x^2) \equiv 1/(1+x^2)^2$ accounts for the proton’s internal structure, $\Lambda_p \simeq 0.77 \text{ GeV}$ [10]. We refer the reader to the Supplemental Material for a brief compendium of the relevant kinematical formulae and a detailed derivation of Eq. (7). The lower extreme of integration $T_p^{\min}(T_\chi)$ is the minimal kinetic energy the proton should have to pass a kinetic energy T_χ to DM. The integral over T_p in Eq. (7) shows little dependence on the upper extreme of integration because the proton spectrum is attenuated at large energies. We find that, for the purpose of our numerical calculations, fixing $T_p^{\max} = 10^8 \text{ GeV}$ is accurate enough.

Using the results for Σ_{DM} obtained in the previous subsection, the parameters in Table I and a typical value $\sigma_{\chi p} = 10^{-30} \text{ cm}^2$, we compute numerically the integrals in Eq. (7) and plot in Fig. 3 the BBDM spectrum for the source TXS 0506+056 for a few DM masses.

Direct detection constraints– BBDM possesses enough energy to leave a signal at direct DM detectors (e.g. XENON1T [4]) as well as neutrino detectors (e.g. MiniBooNE [41] and Borexino [42]). From the top of the atmosphere to the location of the detector, the flux of BBDM will be attenuated due to the scatterings with nucleus N in the air and/or soil [43–46]. After having traveled a distance x in the medium, the DM particle remains with a kinetic energy [10, 46]

$$T_\chi(x) = \frac{2m_\chi T_\chi e^{-x/\ell}}{2m_\chi + T_\chi - T_\chi e^{-x/\ell}}, \quad (9)$$

where $\ell^{-1} = [\sum_N 2m_N m_\chi n_N \sigma_{\chi N} / (m_N + m_\chi)^2]$ is the DM inverse mean free path, with n_N and m_N being the number density and mass of nucleus N in the medium, $\sigma_{\chi N}$ the DM-nucleus cross section. Intuitively, the larger $\sigma_{\chi p}$ is, the more the DM flux is reduced, leading to a blind spot for direct DM detection if $T_\chi(x)$ becomes smaller than the detector’s energy threshold T_{exp}^{\min} . By inverting

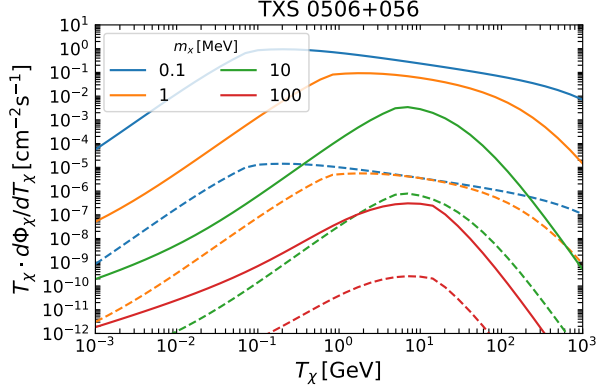


FIG. 3. The expected flux of BBDM from TXS 0506+056. Different colours correspond to different DM mass m_χ , namely 0.1 MeV (blue), 1 MeV (orange), 10 MeV (green), and 100 MeV (red). The solid and dashed lines represent BMP1 and BMP2, respectively. Note that all these results are derived by setting $\sigma_{\chi p} = 10^{-30} \text{ cm}^2$.

Eq. (9) and using the scattering kinematics in Supplemental Material, we approximate the upper limit for $\sigma_{\chi p}$ (dubbed $\sigma_{\chi p}^{\text{upper}}$) as:

$$\sigma_{\chi p}^{\text{upper}} \simeq \log \left[1 + \frac{2m_\chi}{T_\chi^{\min}(T_{\text{exp}}^{\min})} \right] \frac{\sigma_{\chi p} \ell}{x}, \quad (10)$$

where $T_\chi^{\min}(T_{\text{exp}}^{\min})$ is the minimal DM kinetic energy necessary to leave a detectable recoil energy at the direct detector. Note that $\sigma_{\chi p} \ell$ is actually independent of the cross section. A complication arises in the calculation of ℓ . In Ref. [10], the authors use DarkSUSY [47] to calculate the average density n_N of Earth's 11 most abundant elements between the surface and depth x . However, in our work we adopt a more concise and practical approach by using the concept of Meter Water Equivalent (MWE). More specifically, we consider the medium as just composed by water and convert the detector depths in MWE, which for XENON1T, MiniBooNE and Borexino result in 3650 m [48], 26 m [41] and 3800 m [42], respectively. We find that the results of our simplified method are in good agreement with those presented in Ref. [10]. The depth x in the Eq. (10) should include the time-dependence effects of the blazar's position with respect to the detector, but we have verified that, for the two considered sources, these would only slightly affect our final results. Moreover, these effects could eventually be avoided by averaging over the full set of blazars in the entire sky.

On the other hand, if $\sigma_{\chi p}$ is too small, the BBDM flux and the DM-proton scattering can be too weak to leave any recoil in the detectors. Correspondingly, there exists a lower detectable bound on $\sigma_{\chi p}$ which is determined by the detector's sensitivity. Considering an elastic scattering between DM and the target nucleus N and denoting with T_N the nuclear recoil energy, the BBDM induced

target nucleus recoil rate can be expressed as

$$\Gamma_N^{\text{DM}} = \int_{T_{\text{exp}}^{\min}}^{T_{\text{exp}}^{\max}} dT_N \tilde{\sigma}_{\chi N} \int_{T_\chi^{\min}(T_N)}^{+\infty} \frac{dT_\chi}{T_N^{\max}(T_\chi)} \frac{d\Phi_\chi}{dT_\chi}, \quad (11)$$

where $[T_{\text{exp}}^{\min}, T_{\text{exp}}^{\max}]$ is the energy range of sensitivity of the detector and T_N^{\max} is the maximal recoil energy of the nucleus. The nuclear cross section $\tilde{\sigma}_N$ contains the form factor as in Eq. (8). We emphasize that, since $\tilde{\sigma}_{\chi N} \propto \sigma_{\chi p}$ and $d\Phi_\chi/dT_\chi \propto \sigma_{\chi p}$, then $\Gamma_N^{\text{DM}} \propto \sigma_{\chi p}^2$. By comparison with the nucleus recoil limits of different experiments, we can derive the bounds on $\sigma_{\chi p}$. For the spin-independent case, we consider the experiments XENON1T and MiniBooNE. The target nucleus of XENON1T is Xe ($\Lambda_{\text{Xe}} \approx 141 \text{ MeV}$ [49]) and the limiting scattering rate per nucleus is given by

$$\Gamma_{\text{Xe}}(4.9 \text{ keV} \leq T_{\text{Xe}} \leq 40.9 \text{ keV}) < 7.18 \times 10^{-43} \text{ s}^{-1}. \quad (12)$$

For the MiniBooNE experiment, the limiting counting rate per proton is [10]

$$\Gamma_p(T_p > 35 \text{ MeV}) < 1.5 \times 10^{-32} \text{ s}^{-1}. \quad (13)$$

The resulting limits on the spin-independent cross section $\sigma_{\chi p}^{\text{SI}}$ from TXS 0506+056 and BL Lacertae are shown in the upper and lower panels of Fig. 4, respectively. The solid (dashed) lines correspond to BMP1 (BMP2). For each blazar, the difference between solid and dashed lines comes from $\Sigma_{\text{DM}}^{\text{tot}}$ and $\sigma_{\chi p} \propto 1/\sqrt{\Sigma_{\text{DM}}^{\text{tot}}}$. The sensitivity of BBDM is orders of magnitude higher than that of Cosmic Ray Dark Matter (CRDM) [10]. Other complementary limits are also shown for comparison.

For the spin-dependent case, the limiting scattering rate per proton can be derived from proton up-scattering in neutrino detectors like Borexino [42], that is

$$\Gamma_p(T_p > 25 \text{ MeV}) < 2 \times 10^{-39} \text{ s}^{-1}, \quad (14)$$

where we have used the approximation that the ratio between quenched energy deposit (equivalent electron energy T_e) and proton recoil energy T_p fulfills $T_e(T_p)/T_p \approx 2$ for $T_p \gtrsim 5 \text{ MeV}$ [59, 60]. We show the constraints on the spin-dependent cross section $\sigma_{\chi p}^{\text{SD}}$ in Fig. 5. Again, the sensitivities from BBDM are much stronger than that from CRDM.

Conclusion— Due to extremely powerful jets and large DM densities, we find that blazars are ideal DM boosters and can induce a DM flux at Earth stronger than the analogous flux due to the boosting of DM particles in the Milky Way halo by galactic cosmic rays. We have focused on two sample sources, TXS 0506+056 — tentatively identified as a high-energy neutrino source — and the closer BL Lacertae. The limits we have derived from the null detection of the connected DM recoil signal (with DM and neutrino detectors) are the most stringent constraints to date on the DM-proton scattering cross section

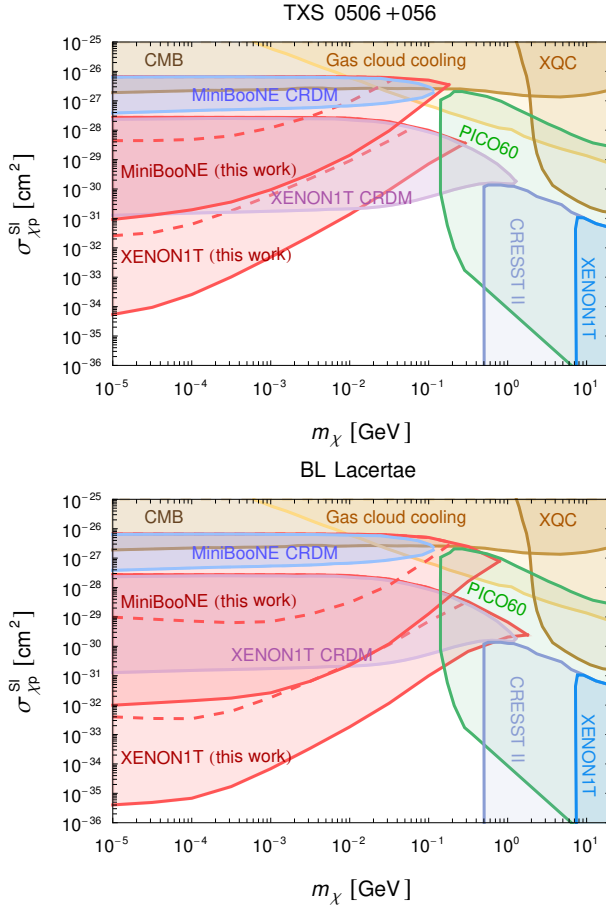


FIG. 4. The constraints on spin-independent DM-proton cross section imposed by XENON1T [4] and MiniBooNE [41]. The red solid and dashed lines correspond to BMP1 and BMP2, respectively. The top panel is for TXS 0506+056, while the bottom for BL Lacertae. For comparison, the constraints from CRDM [10], cosmic microwave background (CMB) observations [50], gas cloud cooling [51], the X-ray quantum calorimeter experiment (XQC) [52], and a selection of direct detection experiments [4, 53–55] are included.

$\sigma_{\chi p}$ for DM masses lighter than about 1 GeV, considering both spin-independent and spin-dependent interactions. The improvement compared to previous results can be as large as 1 up to 5 orders of magnitude, depending on the source and the related uncertainties. While the results presented here rely on assumptions regarding the model of individual blazars and of the associated DM density, we expect that extending the analysis to a full blazar ensemble would eventually allow to significantly reduce the dependence on modelization uncertainties. Indeed, while we are suggesting here a novel method to investigate DM properties, this work could also be relevant to improve the current understanding of blazar jet characteristics.

The authors are grateful to Serguey T. Petcov for useful discussions and helpful suggestions. This work was supported by the research grant “The Dark Uni-

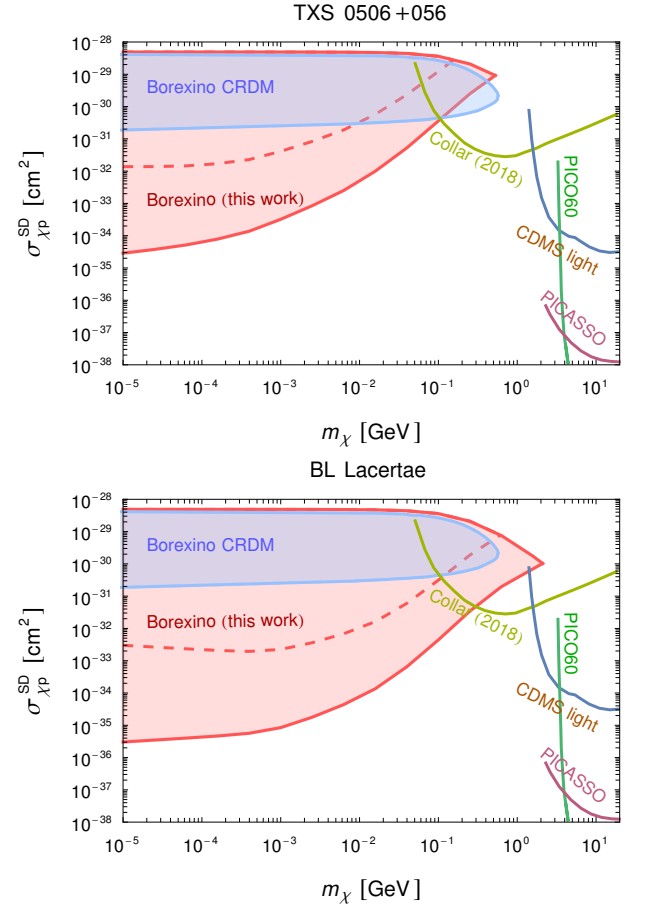


FIG. 5. The constraints on spin-dependent DM-proton cross section imposed by Borexino [42]. The red solid and dashed lines are as in Fig. 4. The top panel is for TXS 0506+056, while the bottom for BL Lacertae. For comparison, we report limits from the direct detection experiments CDMS light [56], PICO60 [55], and PICASSO [57], as well as from delayed-coincidence searches in near-surface detectors by Collar [58].

verse: A Synergic Multi-messenger Approach” number 2017X7X85K under the program PRIN 2017 funded by the The Italian Ministry of Education, University and Research (MIUR), and by the European Union’s Horizon 2020 research and innovation programme under the Marie Skłodowska-Curie grant agreement No 860881-HIDDeN.

* jinwei.wang@sissa.it

† agranell@sissa.it

‡ ullio@sissa.it;

J.-W.W. and A.G. contributed equally to this work.

- [1] G. Bertone, D. Hooper, and J. Silk, Particle dark matter: evidence, candidates and constraints, *Physics Reports* **405**, 279–390 (2005), arXiv:hep-ph/0404175.

- [2] N. Aghanim *et al.* (PLANCK Collaboration), Planck 2018 results, *Astronomy & Astrophysics* **641**, A6 (2020), [arXiv:1807.06209](#).
- [3] E. Aprile *et al.* (XENON1T Collaboration), The XENON1T Dark Matter Search Experiment, *Springer Proc. Phys.* **148**, 93 (2013), [arXiv:1206.6288](#).
- [4] E. Aprile *et al.* (XENON Collaboration), The xenon1t dark matter experiment, *The European Physical Journal C* **77** (2017), [arXiv:1708.07051](#).
- [5] X. Cui *et al.* (PandaX-II Collaboration), Dark Matter Results from 54-Ton-Day Exposure of PandaX-II Experiment, *Physical Review Letters* **119** (2017), [arXiv:1708.06917](#).
- [6] K. Agashe, Y. Cui, L. Necib, and J. Thaler, (in)direct detection of boosted dark matter, *Journal of Cosmology and Astroparticle Physics* **2014** (10), 062–062, [arXiv:1405.7370](#).
- [7] C. Kouvaris, Probing light dark matter via evaporation from the Sun, *Physical Review D* **92** (2015), [arXiv:1506.04316](#).
- [8] H. An, M. Pospelov, J. Pradler, and A. Ritz, Directly Detecting MeV-Scale Dark Matter Via Solar Reflection, *Physical Review Letters* **120** (2018), [arXiv:1708.03642](#).
- [9] T. Emken, C. Kouvaris, and N. G. Nielsen, The Sun as a sub-GeV dark matter accelerator, *Physical Review D* **97** (2018), [arXiv:1709.06573](#).
- [10] T. Bringmann and M. Pospelov, Novel direct detection constraints on light dark matter, *Phys. Rev. Lett.* **122**, 171801 (2019), [arXiv:1810.10543](#).
- [11] C. M. Urry and P. Padovani, Unified schemes for radio-loud active galactic nuclei, *Publications of the Astronomical Society of the Pacific* **107**, 803 (1995), [arXiv:astro-ph/9506063](#).
- [12] A. A. Abdo *et al.*, The Spectral Energy Distribution of Fermi bright blazars, *The Astrophysical Journal* **716**, 30–70 (2010), [arXiv:0912.2040](#).
- [13] L. Maraschi, G. Ghisellini, and A. Celotti, A Jet Model for the Gamma-Ray-emitting Blazar 3C 279, *The Astrophysical Journal* **397**, L5 (1992).
- [14] K. Mannheim, The proton blazar, *Astronomy & Astrophysics* **269**, 67 (1993), [arXiv:astro-ph/9302006](#).
- [15] S. D. Bloom and A. P. Marscher, An Analysis of the Synchrotron Self-Compton Model for the Multi-Wave Band Spectra of Blazars, *The Astrophysical Journal* **461**, 657 (1996).
- [16] A. Mücke and R. Protheroe, A proton synchrotron blazar model for flaring in Markarian 501, *Astroparticle Physics* **15**, 121–136 (2001), [arXiv:astro-ph/0004052](#).
- [17] A. Celotti and G. Ghisellini, The power of blazar jets, *Monthly Notices of the Royal Astronomical Society* **385**, 283–300 (2008), [arXiv:0711.4112](#).
- [18] G. Ghisellini, F. Tavecchio, L. Foschini, G. Ghirlanda, L. Maraschi, and A. Celotti, General physical properties of bright fermi blazars, *Monthly Notices of the Royal Astronomical Society* **402**, 497–518 (2009), [arXiv:0909.0932](#).
- [19] M. Böttcher, A. Reimer, K. Sweeney, and A. Prakash, Leptonic and Hadronic Modeling of Fermi-Detected Blazars, *The Astrophysical Journal* **768**, 54 (2013), [arXiv:1304.0605](#).
- [20] A. A. Abdo *et al.* (Fermi-LAT and MAGIC Collaborations), Insights Into the High-Energy Gamma-ray Emission of Markarian 501 from Extensive Multifrequency Observations in the Fermi Era, *The Astrophysical Journal* **727**, 129 (2011), [arXiv:1011.5260](#).
- [21] A. A. Abdo *et al.* (Fermi-LAT and MAGIC Collaborations), Fermi-LAT Observations of Markarian 421: the Missing Piece of its Spectral Energy Distribution, *The Astrophysical Journal* **736**, 131 (2011), [arXiv:1106.1348](#).
- [22] M. Cerruti, Leptonic and Hadronic Radiative Processes in Supermassive-Black-Hole Jets, *Galaxies* **8**, 72 (2020), [arXiv:2012.13302](#).
- [23] M. Aartsen *et al.* (IceCube, Fermi-LAT, MAGIC, AGILE, ASAS-SN, HAWC, H.E.S.S., INTEGRAL, Kanata, Kiso, Kapteyn, Liverpool telescope, Subaru, Swift/NuSTAR, VERITAS, VLA/17B-403 Collaborations), Multimessenger observations of a flaring blazar coincident with high-energy neutrino IceCube-170922A, *Science* **361** (2018), [arXiv:1807.08816](#).
- [24] M. Aartsen *et al.* (IceCube Collaboration), Neutrino emission from the direction of the blazar TXS 0506+056 prior to the IceCube-170922A alert, *Science* **361**, 147–151 (2018), [arXiv:1807.08794](#).
- [25] P. Padovani, P. Giommi, E. Resconi, T. Glauch, B. Arsioli, N. Sahakyan, and M. Huber, Dissecting the region around IceCube-170922A: the blazar TXS 0506+056 as the first cosmic neutrino source, *Monthly Notices of the Royal Astronomical Society* **480**, 192–203 (2018), [arXiv:1807.04461](#).
- [26] A. Keivani, K. Murase, M. Petropoulou, D. B. Fox, S. B. Cenko, S. Chaty, A. Coleiro, J. J. DeLaunay, S. Dimitrakoudis, P. A. Evans, J. A. Kennea, F. E. Marshall, A. Mastichiadis, J. P. Osborne, M. Santander, A. Tohuvavohu and C. F. Turley, A Multimessenger Picture of the Flaring Blazar TXS 0506+056: Implications for High-energy Neutrino Emission and Cosmic-Ray Acceleration, *The Astrophysical Journal* **864**, 84 (2018), [arXiv:1807.04537](#).
- [27] M. Cerruti, A. Zech, C. Boisson, G. Emery, S. Inoue, and J.-P. Lenain, Leptohadronic single-zone models for the electromagnetic and neutrino emission of TXS 0506+056, *Monthly Notices of the Royal Astronomical Society: Letters* **483**, L12 (2018), [arXiv:1807.04335](#).
- [28] M. Cerruti, A. Zech, C. Boisson, G. Emery, S. Inoue, and J.-P. Lenain, Erratum: Lepto-hadronic single-zone models for the electromagnetic and neutrino emission of TXS 0506+056, *Monthly Notices of the Royal Astronomical Society: Letters* **502**, L21 (2021).
- [29] X. Rodrigues, S. Gao, A. Fedynitch, A. Palladino, and W. Winter, Leptohadronic blazar models applied to the 2014–2015 flare of txs 0506+056, *The Astrophysical Journal* **874**, L29 (2019), [arXiv:1812.05939](#).
- [30] R. Xue, R.-Y. Liu, M. Petropoulou, F. Oikonomou, Z.-R. Wang, K. Wang, and X.-Y. Wang, A two-zone model for blazar emission: Implications for txs 0506+056 and the neutrino event icecube-170922a, *The Astrophysical Journal* **886**, 23 (2019), [arXiv:1908.10190](#).
- [31] M. Petropoulou, K. Murase, M. Santander, S. Buson, A. Tohuvavohu, T. Kawamuro, G. Vasilopoulos, H. Negoro, Y. Ueda, M. H. Siegel, A. Keivani, N. Kawai, A. Mastichiadis and S. Dimitrakoudis, Multi-epoch Modeling of TXS 0506+056 and Implications for Long-term High-energy Neutrino Emission, *The Astrophysical Journal* **891**, 115 (2020), [arXiv:1911.04010](#).
- [32] E. D. Bloom and J. D. Wells, Multi-gev photons from electron–dark-matter scattering near active galactic nuclei, *Physical Review D* **57**, 1299–1302 (1998), [arXiv:astro-ph/9706085](#).
- [33] M. Gorchtein, S. Profumo, and L. Ubaldi, Probing dark

- matter with active galactic nuclei jets, *Phys. Rev. D* **82**, 083514 (2010), [arXiv:1008.2230](#).
- [34] C. D. Dermer and G. Menon, *High Energy Radiation From Black Holes: Gamma Rays, Cosmic Rays, and Neutrinos* (Princeton University Press, 2009).
- [35] J. B. Oke and J. E. Gunn, The Distance of BL Lacertae, *The Astrophysical Journal* **189**, L5 (1974).
- [36] S. Paiano, R. Falomo, A. Treves, and R. Scarpa, The redshift of the bl lac object txs 0506+056, *The Astrophysical Journal* **854**, L32 (2018), [arXiv:1802.01939](#).
- [37] L. Titarchuk and E. Seifina, BL Lacertae: X-ray spectral evolution and a black-hole mass estimate, *Astron. Astrophys.* **602**, A113 (2017), [arXiv:1704.04552](#).
- [38] P. Padovani, F. Oikonomou, M. Petropoulou, P. Giommi, and E. Resconi, TXS 0506+056, the first cosmic neutrino source, is not a BL Lac, *Monthly Notices of the Royal Astronomical Society: Letters* **484**, L104–L108 (2019), [arXiv:1901.06998](#).
- [39] P. Gondolo and J. Silk, Dark matter annihilation at the galactic center, *Phys. Rev. Lett.* **83**, 1719 (1999), [arXiv:astro-ph/9906391](#).
- [40] P. Ullio, H. Zhao, and M. Kamionkowski, A Dark matter spike at the galactic center?, *Phys. Rev. D* **64**, 043504 (2001), [arXiv:astro-ph/0101481](#).
- [41] A. A. Aguilar-Arevalo *et al.* (MiniBooNE Collaboration), The MiniBooNE Detector, *Nucl. Instrum. Meth. A* **599**, 28 (2009), [arXiv:0806.4201](#).
- [42] G. Alimonti *et al.* (Borexino Collaboration), Science and technology of borexino: a real-time detector for low energy solar neutrinos, *Astroparticle Physics* **16**, 205–234 (2002), [arXiv:hep-ex/0012030](#).
- [43] G. D. Starkman, A. Gould, R. Esmailzadeh, and S. Dimopoulos, Opening the Window on Strongly Interacting Dark Matter, *Phys. Rev. D* **41**, 3594 (1990).
- [44] G. D. Mack, J. F. Beacom, and G. Bertone, Towards Closing the Window on Strongly Interacting Dark Matter: Far-Reaching Constraints from Earth’s Heat Flow, *Phys. Rev. D* **76**, 043523 (2007), [arXiv:0705.4298](#).
- [45] D. Hooper and S. D. McDermott, Robust Constraints and Novel Gamma-Ray Signatures of Dark Matter That Interacts Strongly With Nucleons, *Phys. Rev. D* **97**, 115006 (2018), [arXiv:1802.03025](#).
- [46] T. Emken and C. Kouvaris, How blind are underground and surface detectors to strongly interacting Dark Matter?, *Phys. Rev. D* **97**, 115047 (2018), [arXiv:1802.04764](#).
- [47] T. Bringmann, J. Edsjö, P. Gondolo, P. Ullio, and L. Bergström, DarkSUSY 6 : An Advanced Tool to Compute Dark Matter Properties Numerically, *JCAP* **07**, 033, [arXiv:1802.03399](#).
- [48] R. Harnik, R. Plestid, M. Pospelov, and H. Ramani, Millicharged cosmic rays and low recoil detectors, *Phys. Rev. D* **103**, 075029 (2021), [arXiv:2010.11190](#).
- [49] I. Angeli, A consistent set of nuclear rms charge radii: properties of the radius surface $r(n,z)$, *Atomic Data and Nuclear Data Tables* **87**, 185 (2004).
- [50] W. L. Xu, C. Dvorkin, and A. Chael, Probing sub-GeV Dark Matter-Baryon Scattering with Cosmological Observables, *Phys. Rev. D* **97**, 103530 (2018), [arXiv:1802.06788](#).
- [51] A. Bhoonah, J. Bramante, F. Elahi, and S. Schon, Calorimetric Dark Matter Detection With Galactic Center Gas Clouds, *Phys. Rev. Lett.* **121**, 131101 (2018), [arXiv:1806.06857](#).
- [52] M. S. Mahdawi and G. R. Farrar, Constraints on Dark Matter with a moderately large and velocity-dependent DM-nucleon cross-section, *JCAP* **10**, 007, [arXiv:1804.03073](#).
- [53] G. Angloher *et al.* (CRESST Collaboration), Results on MeV-scale dark matter from a gram-scale cryogenic calorimeter operated above ground, *Eur. Phys. J. C* **77**, 637 (2017), [arXiv:1707.06749](#).
- [54] G. Angloher *et al.* (CRESST Collaboration), Results on light dark matter particles with a low-threshold CRESST-II detector, *Eur. Phys. J. C* **76**, 25 (2016), [arXiv:1509.01515](#).
- [55] C. Amole *et al.* (PICO Collaboration), Dark Matter Search Results from the PICO-60 C_3F_8 Bubble Chamber, *Phys. Rev. Lett.* **118**, 251301 (2017), [arXiv:1702.07666](#).
- [56] R. Agnese *et al.* (SuperCDMS Collaboration), Low-mass dark matter search with CDMSlite, *Phys. Rev. D* **97**, 022002 (2018), [arXiv:1707.01632](#).
- [57] E. Behnke *et al.*, Final Results of the PICASSO Dark Matter Search Experiment, *Astropart. Phys.* **90**, 85 (2017), [arXiv:1611.01499](#).
- [58] J. I. Collar, Search for a nonrelativistic component in the spectrum of cosmic rays at Earth, *Phys. Rev. D* **98**, 023005 (2018), [arXiv:1805.02646](#).
- [59] J. F. Beacom, W. M. Farr, and P. Vogel, Detection of Supernova Neutrinos by Neutrino Proton Elastic Scattering, *Phys. Rev. D* **66**, 033001 (2002), [arXiv:hep-ph/0205220](#).
- [60] B. Dasgupta and J. F. Beacom, Reconstruction of supernova ν_μ , ν_τ , anti- ν_μ , and anti- ν_τ neutrino spectra at scintillator detectors, *Phys. Rev. D* **83**, 113006 (2011), [arXiv:1103.2768](#).
- [61] C. V. Cappiello, K. C. Y. Ng, and J. F. Beacom, Reverse direct detection: Cosmic ray scattering with light dark matter, *Phys. Rev. D* **99**, 063004 (2019), [arXiv:1810.07705](#).

Direct Detection Constraints on Blazar-Boosted Dark Matter

Supplemental Material

Jin-Wei Wang, Alessandro Granelli and Piero Ullio

Scuola Internazionale Superiore di Studi Avanzati (SISSA), via Bonomea 265, 34136 Trieste, Italy

INFN, Sezione di Trieste, via Valerio 2, 34127 Trieste, Italy

Institute for Fundamental Physics of the Universe (IFPU), via Beirut 2, 34151 Trieste, Italy

In this Supplemental Material, we first describe how to derive the jet spectrum in the observer's frame. We then report the kinematical formulae for a generic elastic scattering and present a more detailed derivation of the Blazar-Boosted Dark Matter (BBDM) flux, as given in Eq. (7) of the main text.

Jet spectrum in the observer's frame– Consider a jet particle with mass m and energy E in the observer's frame, moving in the direction of polar angle θ and azimuth ϕ with respect to the jet axis. The boost factor ($\gamma = E/m$) and polar angle in the blob frame can be derived from a Lorentz transformation:

$$\gamma'(\gamma, \mu) = (1 - \beta_B \beta \mu) \gamma \Gamma_B, \quad (15)$$

$$\mu'(\gamma, \mu) = \frac{\beta \mu - \beta_B}{\sqrt{(1 - \beta_B \beta \mu)^2 - (1 - \beta^2)(1 - \beta_B^2)}}, \quad (16)$$

where $\beta = \sqrt{1 - 1/\gamma^2}$ is the velocity of the particle. In our notation the variables with and without a prime are computed in the blob and observer's frame, respectively. We define the number of particles injected by the blazar per unit time, per unit energy and per unit solid angle as $d\Gamma/(dEd\Omega)$ (dubbed spectrum). The spectrum in the observer's frame can be obtained by boosting it from the blob frame. Following similar steps as the ones presented in Ref. [33], we arrive to

$$\begin{aligned} \frac{d\Gamma}{dEd\Omega} &= \Gamma_B \frac{d\Gamma'}{dE'd\Omega'} \left| \det \begin{pmatrix} \frac{\partial \gamma'}{\partial \gamma} & \frac{\partial \gamma'}{\partial \mu} \\ \frac{\partial \mu'}{\partial \gamma} & \frac{\partial \mu'}{\partial \mu} \end{pmatrix} \right| \\ &= \frac{d\Gamma'}{dE'd\Omega'} \frac{\beta}{\sqrt{(1 - \beta \beta_B \mu)^2 - (1 - \beta^2)(1 - \beta_B^2)}}. \end{aligned} \quad (17)$$

It is straightforward to verify that, for a spectrum in the blob frame, e.g. a single power-law distribution, the spectrum of protons can be reduced to the form given in Eq. (2) of the main text.

Elastic scattering kinematics– For an elastic scattering process $i, j \rightarrow i, j$, where i, j denote particles with mass $m_{i,j}$. In the main text we consider the case in which $i, j \in \{\chi, p, N\}$. In the laboratory (LAB) frame, we assume that j is effectively at rest. After a scattering, the kinetic energy (or recoil energy) T_j transferred to the particle j from the incoming particle i with kinetic energy T_i is [10, 61]

$$T_j = T_j^{\max} \frac{1 + \mu_s^*}{2} \quad \text{with} \quad T_j^{\max}(T_i) = \frac{(T_i^2 + 2m_i T_i)}{T_i + (m_i + m_j)^2/(2m_j)}, \quad (18)$$

where μ_s^* is the cosine of the scattering angle in the CM rest frame. Inverting Eq. (18) gives the

minimal energy the particle i should have to pass a kinetic energy T_j to particle j [10]:

$$T_i^{\min}(T_j) = \frac{1}{2} \left[(T_j - 2m_i) \pm \sqrt{(T_j - 2m_i)^2 + 2(m_i + m_j)^2 T_j / m_j} \right], \quad (19)$$

where the $+$ ($-$) applies for $T_j \geq 2m_i$ ($T_j < 2m_i$). Lorentz transformations relate the scattering angles in the LAB and CM frames via:

$$\mu_s^* = \frac{2\mu_s^2}{\mu_s^2 + \gamma_{\text{CM}}^2(T_i)(1 - \mu_s^2)} - 1, \quad (20)$$

where

$$\gamma_{\text{CM}}^2(T_i) \equiv \frac{(T_i + m_i + m_j)^2}{(m_i + m_j)^2 + 2m_j T_i}. \quad (21)$$

Using Eq. (20) and assuming an isotropic collision in the CM frame, we can derive the probability distribution of the DM scattering angle in the LAB frame:

$$P(\mu_s; T_i) \equiv \frac{1}{2} \frac{d\mu_s^*}{d\mu_s} = \frac{2\mu_s \Theta(1 - \mu_s)}{[\mu_s^2 + \gamma_{\text{CM}}^2(T_i)(1 - \mu_s^2)]^2}. \quad (22)$$

where the Heaviside theta function ensures that $0 \leq \mu_s \leq 1$. The kinetic energy of the outgoing particle j in terms of the scattering angle in the LAB frame is then given by:

$$T_j(T_i, \mu_s) = T_j^{\max}(T_i) \frac{\mu_s^2}{\mu_s^2 + \gamma_{\text{CM}}^2(T_i)(1 - \mu_s^2)}. \quad (23)$$

Inverting Eq. (23), we obtain the scattering angle that corresponds to an incoming kinetic energy T_i and transferred energy T_j :

$$\bar{\mu}_s(T_i, T_j) = \left[1 + \frac{T_j^{\max}(T_i) - T_j}{T_j \gamma_{\text{CM}}^2(T_i)} \right]^{-1/2}. \quad (24)$$

BBDM flux at Earth – We now briefly explain how to derive the BBDM flux as given in Eq. (7) of the main text. We make use of the kinematic formulae presented above using $i = p$ and $j = \chi$ and consider the LAB frame to coincide with the observer's frame, i.e. we neglect the motion of dark matter with respect to the protons. Assuming the elastic cross section to be isotropic in the CM rest frame, the flux per kinetic energy of BBDM can be written as

$$\frac{d\Phi_\chi}{dT_\chi} = \frac{\Sigma_{\text{DM}}^{\text{tot}} \tilde{\sigma}_{\chi p}}{m_\chi d_L^2} \int_0^{2\pi} d\phi_s \int_0^1 d\mu_s \int_{T_p^{\min}(T_\chi)}^{T_p^{\max}(T_\chi)} dT_p \frac{d\Gamma_p}{dT_p d\Omega} \frac{P(\mu_s, T_p)}{2\pi} \delta(T_\chi - T_\chi(T_p, \mu_s)) \quad (25)$$

where $\phi_s \in [0, 2\pi]$ is the azimuthal angle with respect to the LOS. $T_\chi(T_p, \mu_s)$ is the dark matter kinetic energy after scattering for given T_p and μ_s . Note that the proton spectrum depends on μ , which is related to μ_s and ϕ_s by a rotation of an angle θ_{LOS} , namely

$$\mu(\mu_s, \phi_s) = \mu_s \cos \theta_{\text{LOS}} + \sin \phi_s \sin \theta_{\text{LOS}} \sqrt{1 - \mu_s^2}. \quad (26)$$

Using the properties of the Dirac δ -function we can write:

$$\delta(T_\chi - T_\chi(T_p, \mu_s)) = \frac{\delta(\mu_s - \bar{\mu}_s(T_p, T_\chi))}{T_\chi^{\max}(T_p) P(\mu_s; T_p)}, \quad (27)$$

Therefore, the flux can be rewritten as:

$$\frac{d\Phi_\chi}{dT_\chi} = \frac{\Sigma_{\text{DM}}^{\text{tot}} \tilde{\sigma}_{\chi p}}{2\pi m_\chi d_L^2} \int_0^{2\pi} d\phi_s \int_{T_p^{\min}(T_\chi)}^{T_p^{\max}} \frac{dT_p}{T_\chi^{\max}(T_p)} \frac{d\Gamma_p}{dT_p d\Omega}, \quad (28)$$

where the proton spectrum needs to be evaluated at $\mu(\bar{\mu}_s(T_p, T_\chi), \phi_s)$. We note that, in the case of $\theta_{\text{LOS}} = 0$, $\mu = \mu_s$ and therefore the integration over ϕ_s in Eq. (28) becomes trivial.